Journal of Thermal Analysis and Calorimetry, Vol. 91 (2008) 2, 581–587

CuO NANOCRYSTALS IN THERMAL DECOMPOSITION OF AMMONIUM PERCHLORATE
Stabilization, structural characterization and catalytic activities

*L.-J. Chen, G.-S. Li and L.-P. Li**

State Key Lab of Structural Chemistry, Fujian Institute of Research on the Structure of Matter and Graduate School of the Chinese Academy of Sciences, Fuzhou 350002, P. R. China

CuO nanocrystals of different surface areas were prepared. All samples were characterized by X-ray diffraction, transition electron microscope, thermogravimetry, Brunauer–Emmett–Teller technique, Fourier transform infrared spectroscopy, and Raman spectroscopy. CuO nanocrystals showed a stable monoclinic structure. With increasing surface areas, the surface hydration became significant, which is followed by shifts in infrared frequencies and Raman phonon modes. CuO nanocrystals were explored as an additive to catalytic decomposition of ammonium perchlorate (AP). AP decomposition underwent a two-stage process. Addition of CuO nanocrystals led to a downshift of high-temperature stage towards lower temperatures.

Keywords: *ammonium perchlorate, catalytic activity, CuO nanocrystals, thermal decomposition*

Introduction

CuO is a typical p-type semiconductor with a narrow bandgap of 1.2 eV and has promising applications in many fields including catalyst [1], lithium ion batteries [2], magnetic storage [3], semiconductors [4], gas sensor [5], and solar-energy conversion [6]. The performance of CuO in these applications can be significantly improved when the particle sizes are controlled to vary within the nanoscale regime. For instance, the catalytic activities of nanocrystals are superior over the bulk in the thermal decomposition of ammonium perchlorate (AP) [7].

AP is one of the main oxidizing agents in composite solid propellants, in which AP plays a significant role in the burning process [8]. Thermal decomposition of AP has been extensively studied by taking advantages of the catalytic activities of additives of transition metal oxides and metal powders [9, 10]. It is shown that among these catalytic additives, CuO nanocrystals could be an effective catalyst during AP decomposition, though their physical dimension dependences of catalytic activities are still poorly understood. Luo *et al.* thought the average size of CuO has no influence on the thermal decomposition of AP [11], while Singh *et al.* concluded that CuO with larger surface areas can give higher catalytic activity towards the AP decomposition [12]. A systematic study of the effects of different sizes (or surface areas) of CuO nanocrystals additives on AP decomposition is necessary to understand the underlying catalysis.

Material stabilization is also a great concern to the catalytic and many other applications of CuO nanocrystals. Palkar *et al*. prepared CuO nanocrystals by annealing the dehydrated citrate precursor and freshly precipitated oxalate [13]. They found that CuO nanocrystals were unstable below 25 nm and would transform into high-symmetry cubic Cu_2O. Alcohol-thermal method is facile to synthesize small size of about 3 nm CuO [14], but during the subsequent high temperature reaction, CuO nanocrystals are always partially reduced to Cu_2O or Cu nanocrystals by ethanol. Consequently, controlled growth of CuO nanocrystals under an oxidation condition at low temperature is expected to give high quality nanocrystals for phase stabilization and large surface areas, which can provide some information relating to the fundamental issues of the physical properties and catalytic activities in thermal decomposition of AP.

In this paper, we used a simple combined methodology involving water-ethanol solvents to stabilize CuO nanocrystals with a BET surface of 76.5 $m^2\ g^{-1}$. We explored a kinetic control over the surface areas by high temperature calcinations. Depending on the surface areas, CuO nanocrystals showed significant variations in lattice dimension and phonon mode frequencies. When taking as a catalytic additive, CuO nanocrystals promoted the thermal decomposition of AP significantly with increasing surface areas.

* Author for correspondence: lipingli@fjirsm.ac.cn

1388–6150/$20.00

Akadémiai Kiadó, Budapest, Hungary
Springer, Dordrecht, The Netherlands

Experimental

Chemical reagents of $Cu(NO_3)_2 \cdot 3H_2O$ and NaOH were used as the starting materials. At room temperature, 400 mL of 0.25 M $Cu(NO_3)_2 \cdot 3H_2O$ in ethanol was slowly added into 200 mL of 1.25 M NaOH in ethanol under stirring in a flask to form a black precipitate. 200 mL water was then added to this mixture. After ageing for 8 h at room temperature, the precipitated product was washed fully with distilled water and dried in an oven at 100°C for 6 h. The powder obtained was named as as-prepared sample. CuO nanocrystals were achieved to have different surface areas by annealing as-prepared sample at given temperatures at 300, 350, 400, 450 and 700°C for 4 h in a flowing O_2 atmosphere.

The structures of the samples were examined by powder X-ray diffraction using Rigaku DMAX2500 X-ray diffractometer with monochromatized CuK_α radiation (λ=0.15418 nm). The lattice parameters were refined by using Retica Rietveld program with peak positions that are calibrated by internal standard of silica (99.9% pure). The particle sizes and morphologies of the samples were determined using TEM on a JEM-2010 apparatus with an acceleration voltage of 200 kV. The specific surface areas of CuO nanocrystals were determined from the nitrogen absorption data at liquid nitrogen temperature using BET technique on a Micromeritics ASAP 2000 Surface Area and Porosity Analyzer. Thermal behaviors of the samples were carried out using thermogravimetric analysis at a heating rate of 15°C min^{-1} from room temperature to 1100°C in a N_2 atmosphere and under ambient atmospheric pressure. Infrared spectra of the samples were recorded with PerkinElmer IR spectrophotometer using the KBr pellet technique. Raman spectra were recorded using a JY-HR800 spectrometer with a He-Ne laser. The excitation wavelength is 632.8 nm and output powder is 20 mW.

The catalytic activities of CuO nanocrystals in the thermal decomposition of AP (180 μm) were also studied using the STA449C thermal analyzer at a heating rate of 20°C min^{-1} in N_2 atmosphere over the range of 30–500°C. TG experiments were performed using open alumina crucible. AP and CuO nanocrystals were mixed at a mass ratio of 98:2 to prepare the target samples for thermal decomposition analyses. A total sample mass of 1.5 mg was used in all runs.

Results and discussion

Figure 1 shows the XRD patterns for as-prepared sample and CuO nanocrystals obtained after calcinations at given temperatures. The diffraction peaks of as-prepared sample are essentially identical to the

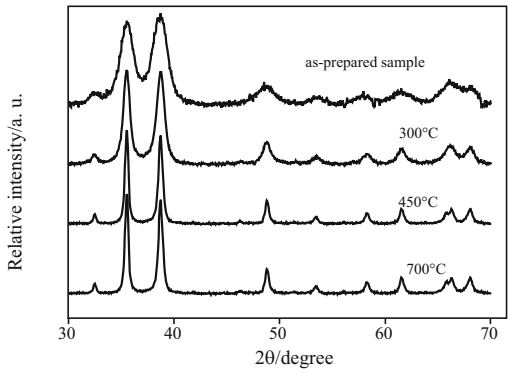

Fig. 1 XRD patterns of CuO nanocrystals that were obtained after calcinations at given temperatures. Vertical bars represent the standard diffraction data from JPCDS file for CuO (No. 05-0661)

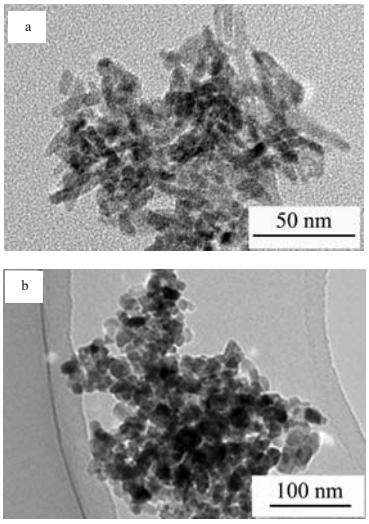

Fig. 2 TEM images of a – as-prepared CuO nanocrystals and b – those obtained after calcinations at 300°C

standard data for CuO (JCPDS No. 05-0661), while no impurity peaks such as those from $Cu(OH)_2$ or Cu_2O were observed. All these demonstrated the formation of monoclinic CuO nanocrystals. The formation reaction of as-prepared sample probably proceeded through a rapid dehydration of $Cu(OH)_2$ in a water-alcohol solvent system. TEM images of as-prepared CuO nanocrystals and those after annealing at 300°C are shown in Fig. 2. It is seen that the as-prepared CuO nanocrystals consisted of nanorods, which transformed into spherical particles after annealing. With increasing the annealing temperature, XRD line width became systematically narrowed (Fig. 1).

Particle sizes calculated from XRD line broadening are not always accurate in particular for the present CuO nanorods because many factors such as the size of coherent diffraction domains, strains, and lattice distortions may be involved. In the following, we will address the size effects of CuO nanocrystals using the surface areas.

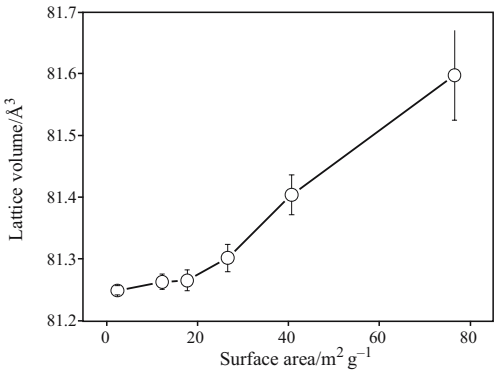

Fig. 3 Lattice volume of CuO nanocrystals as a function of surface areas

The surface areas of CuO nanocrystals were measured by BET technique. The as-prepared CuO nanocrystals gave a large surface area of 76.5 m^2 g^{-1}. With increasing the treatment temperatures, surface areas became smaller, e.g., 40.7 m^2 g^{-1} (300°C), 26.6 m^2 g^{-1} (350°C), 17.7 m^2 g^{-1} (400°C), 12.2 m^2 g^{-1} (450°C), and 2.4 m^2 g^{-1} (700°C). As for many nanocrystals, the variations of surface area would usually change the structural stability and equivalent lattice dimension [15]. The lattice parameters of CuO nanocrystals were obtained by structural refinements using Retica Rietveld program. Figure 3 shows the relationship between the lattice volume and surface areas of CuO nanocrystals. It is seen that when surface areas are increased from 2.4 to 76.5 m^2 g^{-1}, the lattice volume increased from 81.25 to 81.60 Å^3. The magnitude of lattice expansion is smaller than that reported by Punnoose *et al.* [16], which demonstrates the low concentration of lattice defects in our CuO nanocrystals. With regards to the lattice expansion that occurs within the nanoscale regime, two primary factors have to be taken into account, namely, valence reduction and surface dipole-dipole interactions. Valence reduction can give rise to a lattice expansion because lower valence ions generally have larger ionic sizes. Palkar *et al*. [13] characterized the CuO nanocrystals obtained by annealing citrate precursors and oxalates, and found that the resulting CuO nanocrystals contained certain amounts of Cu^+. For the present CuO nanocrystals, the occurrence of Cu^+ from the reduction of Cu^{2+} can be eliminated during the dehydration process of $Cu(OH)_2$ since high concentration of sodium hydroxide in ethanol solution could significantly accelerate the decomposition of $Cu(OH)_2$ [17]. The oxygen atmosphere used during the calcinations could also suppress the reduction of Cu^{2+}. Therefore, the mixed valence of Cu^{2+} and Cu^+ can be excluded as a cause of the distinct structural stability and lattice variations in CuO nanocrystals.

Surface dipole-dipole interactions can give rise to a strong negative pressure for the lattice expansion [16]. To understand these strong interactions, it is essential to examine the surface hydration chemistry since the large surfaces of nanocrystals are highly reactive to adsorbed water in changing the surface energies by forming hydration layers and since the existence of hydration layer can affect many properties of nanocrystals [18]. The thermal behaviors of CuO nanocrystals were investigated by TG technique. Figure 4a illustrates the TG data of CuO nanocrystals with different surface areas. From Fig. 4a, it is seen that CuO nanocrystals underwent a continuous mass loss (<400°C) and a sharp mass loss (>900°C). With regards to the continuous mass loss, the thermal effect that occurred at temperatures below 100°C is associated with the physisorbed water, while that at temperatures higher than 100°C is due to dehydration of the chemisorbed water. When temperature was increased higher than 900°C, the relative mass loss is almost a constant (about 9.67%), which is associated with the reduction reactions from CuO to Cu_2O and a release of oxygen. Figure 4b shows the mass losses of CuO as a function of surface areas in comparison with those of the CuO nanocrystals prepared directly from hydrothermal conditions [19]. It is seen that the surface water contents of CuO nanocrystals increased with surface area, regardless of the preparation methods. Nevertheless, the surface water contents for the pres-

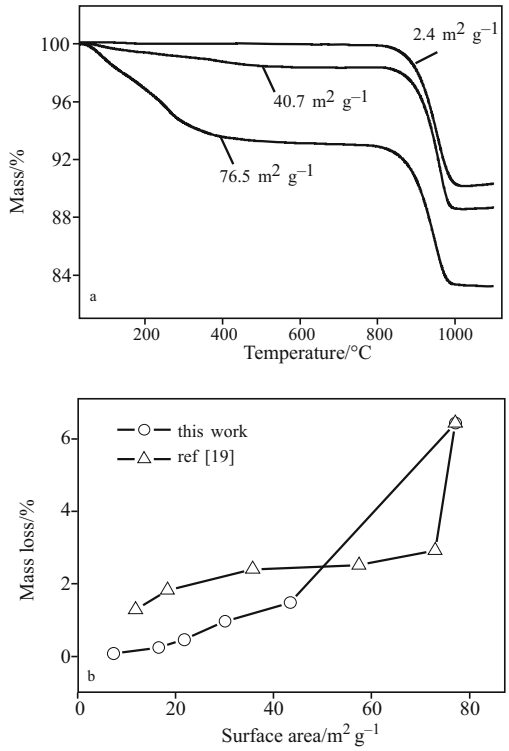

Fig. 4 a – TG data of CuO nanocrystals of given surface areas and b – mass losses of absorbed water as a function of surface areas. Reference data of CuO nanocrystals prepared directly by hydrothermal method [19] were also given for comparison

ent CuO nanocrystals are slightly smaller than those prepared directly by hydrothermal conditions, which indicates a distinct surface hydration configuration. It is well known that the surface hydration can lead to a significant decrease in surface energies [20]. Therefore, the water layers formed on the surface of CuO nanocrystals can partially balance the dipole-dipole interactions and further yield surface structure relaxation and changes in lattice dimensions. Since particle size reduction is generally followed by a larger surface to volume ratio, broken lattice symmetry, and a high concentration of unsaturated bonds on surfaces, vibrational properties of CuO nanocrystals can be varied depending on the surface areas.

Vibrational properties of CuO nanocrystals were studied by IR and Raman spectra. CuO belongs to the C_{2h}^6(C 2/c) space group with two molecules involving in a primitive cell. Therefore, there are 12 vibration modes, in which six modes are infrared active, three are acoustic modes, and three are Raman active. Figure 5a shows infrared spectrum of CuO nanocrystals with a surface area of 76.5 m^2 g^{-1}. Besides the strong absorptions at 3420 and 1624 cm^{-1} for surface hydration and those at 1471, 1358, 847 and 779 cm^{-1} for CO_3^{2-} and HCO_3^- ions, three complex peaks centered at 429, 502 and 591 cm^{-1} were observed. According to the assignments in literature [21], both absorption bands located at about 502 and 429 cm^{-1} are associated with the transverse optical vibration modes (TO), while the absorption at 591 cm^{-1} is associated with longitudinal optical vibration mode (LO). As indicated by the enlarged infrared spectra of CuO nanocrystals (Fig. 5b), with decreasing surface areas from 76.5 to 2.4 m^2 g^{-1}, TO modes shifted towards lower frequencies with a shift of about 31 and 50 cm^{-1}, respectively (see dashed line in Fig. 5b), while the LO mode showed a slight red shift of about 9 cm^{-1}. To understand the nature of these abnormal vibrational properties, it is essential to recall the force constant model.

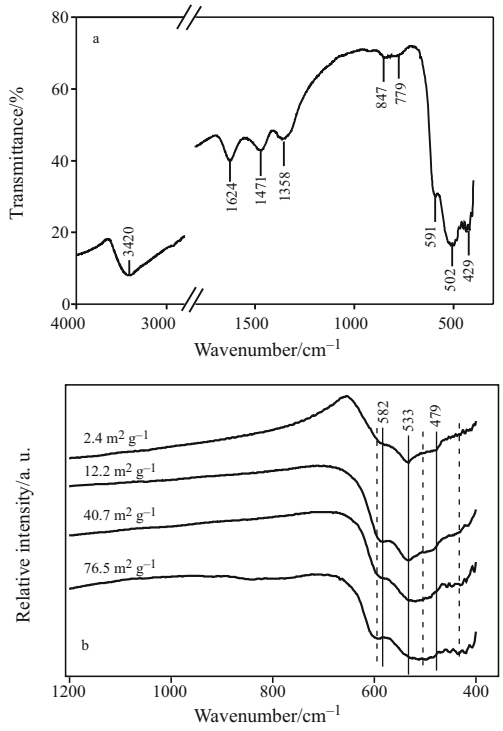

Fig. 5 a – Infrared spectrum of CuO nanocrystals with a surface area of 76.5 m^2 g^{-1}, and b – enlarged infrared spectra of CuO nanocrystals of given surface areas

According to this model, the frequencies of lattice vibrations are a function of the lattice dimension and bonding nature. Investigations on many oxide nanocrystals have concluded that the lattice expansion is generally followed by an increase in ionicity of metal-oxide bond [13]. The nature of chemical bonding between metal and oxygen in oxide lattice can be measured by the frequency difference, Δ(TO–LO), between transverse and longitudinal optical vibration modes. For the present CuO nanocrystals, the values for Δ(TO–LO) is increased by 40 or 59 cm^{-1} with increasing surface areas, which indicates the ionicity enhancement of chemical bonds of Cu–O in CuO nanocrystals. Similar results have been reported in spinel oxide materials [22].

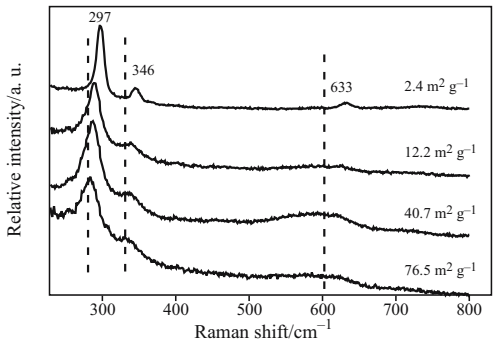

Fig. 6 Raman spectra of CuO nanocrystals of given surface areas

Figure 6 shows the Raman spectra of CuO nanocrystals of different surface areas. Three peaks at about 297, 346 and 633 cm^{-1} were observed for CuO. The peak at 297 cm^{-1} is assigned to A_g mode, and peaks at 346 and 633 cm^{-1} to B_g modes [23]. With increasing the surface areas, Raman peaks showed a decrease in peak intensity, broadened width, lowered frequency (Fig. 6). According to the formula of Gruneisen constant, $\gamma = -d\ln\omega/d\ln V$, the shift of Raman peaks is associated with the variations in lattice dimension via the following equation:

$$\Delta\omega = -\gamma\omega_0 \frac{\Delta V}{V_0} \quad (1)$$

where γ is the Gruneisen constant, ω_0 is the Raman peak position of the bulk, V_0 is the lattice volume of the bulk, and ΔV is the variation of lattice volume under the external fields such as high pressures. The values of γ are all positive for these three modes (one A_g mode and two B_g modes) of CuO [24]. As shown in Fig. 3, for the present work, ΔV is positive as the lattice dimension increased with increasing surface areas. All these explain the frequency shift of the phonon modes towards lower frequencies at larger surface areas.

The confinement effect is another important factor that influences the Raman spectrum. The first-order Raman spectrum $I(w)$ can be described as follows [25]:

$$I(w)=\int \frac{|C(0,k)|^2}{[w-w(k)]^2+(\Gamma_2/2)^2}\mathrm{d}^3k \qquad (2)$$

where $w(k)$ is the phonon dispersion relation, Γ_0 is the natural full line width, and $c(0,k)$ is the Fourier coefficient that describes the phonon confinement which can be written as:

$$|C(k)|=\exp(-k^2L^2/16\pi^2) \qquad (3)$$

where L is the average size of nanocrystals. As the particle size is reduced into the nanoscale regime, the large effect on the Raman peaks is the crystal momentum conservation rules. This allows phonons with wave vector $|k|=|k'|\pm 2\pi/L$ to participate in the first-order Raman scattering [26] (k' is the wave vector of the incident light). The phonon dispersion near the zone center has to be considered since the phonon scattering will not be limited to the center of the Brillouin zone. As a result, the Raman spectra are broadened and downshifted as increasing surface areas.

Large surface areas always contribute to the catalytic activities. Here, we investigated the surface area dependence of the catalytic activities of CuO nanocrystals by TG-DTA. TG curves for pure AP and mixtures of AP with CuO nanocrystals of different surface areas are shown in Fig. 7. The decomposition of pure

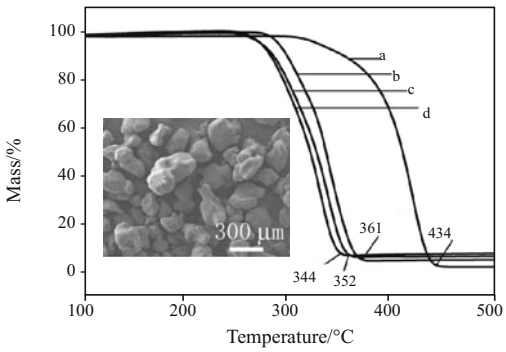

Fig. 7 TG curves for: a – pure AP, b – AP+CuO (2.4 $m^2\ g^{-1}$), c – AP+CuO (40.7 $m^2\ g^{-1}$), and d – AP+CuO (76.5 $m^2\ g^{-1}$). Inset shows the SEM image of AP

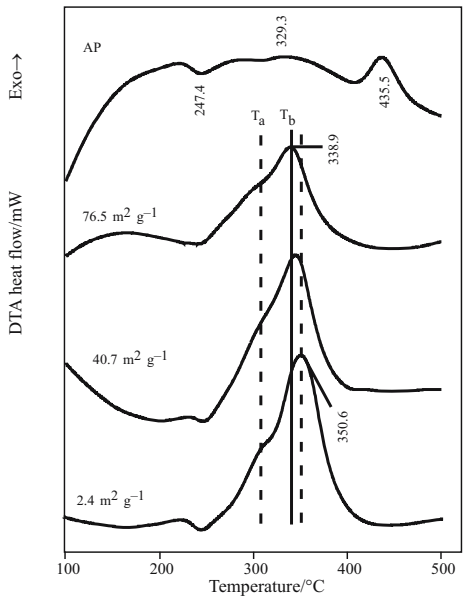

Fig. 8 DTA curves of pure AP and mixtures of AP with CuO nanoparticles of given surface areas

AP is generally centered at temperatures from 329 to 434°C. Addition of CuO nanocrystals in AP led to a significant reduction of the ending decomposition temperature of AP. With increasing the surface area from 2.4 to 76.5 $m^2\ g^{-1}$, the ending decomposition temperatures of AP decreased from 361 to 344°C.

Figure 8 shows the differential thermal analysis (DTA) curves of pure AP and mixtures of AP with CuO nanoparticles of given surface areas. For pure AP, an endothermic peak was observed at about 250°C, which is assigned to the crystallographic transition of AP from orthorhombic to cubic [10]. With increasing the temperatures, AP underwent two complicated decomposition stages [10], i.e., a low temperature stage at 329.3°C and a high temperature stage at 435.5°C, which are followed by two exothermic peaks. These two decomposition stages are consistent with those of 80 μm AP but are apparently different from the single step for 1.1 μm AP [10]. Such an observation clearly indicates a size effect since as indicated by SEM image in inset of Fig. 7, AP used in this work has a large particle size of 180 μm. All CuO nanocrystals have no significant impacts on the phase transition of AP and low-temperature decomposition stage of AP (T_a as shown in Fig. 8), but the high-temperature decomposition stage of AP (T_b as shown in Fig. 8). With increasing the surface area from 2.4 to 76.5 $m^2\ g^{-1}$, the high-temperature decomposition stage showed a downshift from 84.9 to 96.6°C. The significant surface area dependence of catalytic activity of CuO nanocrystals in AP decomposition discovered in this work is different from the previous literature report [11], since for the latter case, particle sizes are concluded to have no impacts on the catalytic ac-

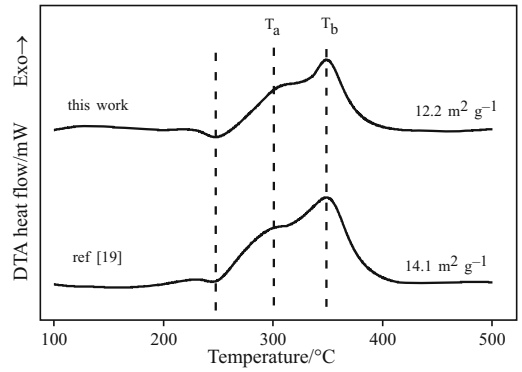

Fig. 9 DTA curve for the as-prepared CuO nanocrystals with a surface area of 12.2 m^2 g^{-1}. For comparison, DTA data of the samples of similar surface area that were prepared directly by hydrothermal conditions [19] were also given

tivities. On the other hand, the catalytic activities of nanostructure CuO is superior over the nanostructure Ni or Al, which only slightly lowers the peak temperature of the high-temperature decomposition stage [10]. Apparently, large surface areas of CuO nanocrystals played the key role in enhancing the catalytic activities in the thermal decomposition of AP, which is probably because the high-temperature thermal decomposition stage of AP takes place on the surface including the adsorption and desorption of surface species [27].

As stated above, large surface areas also give rise to a significant surface hydration. To investigate the influence of surface hydration on the catalytic activities of AP, we compared the DTA curves for the samples of this work with those of similar surface areas [19] prepared directly by hydrothermal method. As illustrated in Fig. 9, the water contents on both samples are different: the as-prepared sample had a water content of 0.32 W%, which is 6 times lower than that of 2% when sample was prepared using hydrothermal conditions. Interestingly, the high-temperature decomposition stage (T_b as shown in Fig. 9) in presence of these two samples remained almost the same. Therefore, the surface hydration on the samples has no apparent impacts on the thermal decomposition of AP.

Conclusions

This work reported on the stabilization, structural characteristics, and catalytic activities of CuO nanocrystals. CuO nanocrystals were prepared to have distinct surface areas by high temperature treatments. All CuO nanocrystals were terminated with surface hydration. With increasing the surface areas, surface hydration became significant, which is followed by shifts and broadening of Raman and infrared spectra. The changes in surface areas did not alter the structural stabilities of CuO nanocrystals, instead, the lattice dimension became increased with surface areas owing to the positive Gruneisen parameters. Depending on the surface areas, CuO additives enhanced the thermal decomposition of AP, while the impacts of surface hydration could be ignored.

Acknowledgements

This work was financially supported by NSFC under the contract (No.20671092), Science and Technology Program from Fujian Province (No. 2005HZ01-1), a grant from Hundreds Youth Talents Program of CAS (Li GS), and in part by Research Foundation for the Returned Overseas Chinese scholars, State Education Ministry.

References

1 R. Prasad, J. Therm. Anal. Cal., 85 (2006) 279.
2 X. P. Gao, J. L. Bao, G. L. Pan, H. Y. Zhu, P. X. Huang, F. Wu and D. Y. Song, J. Phys. Chem. B., 108 (2004) 5547.
3 R. V. Kumar, Y. Diamant and A. Gedanken, Chem. Mater., 12 (2000) 2301.
4 E. M. Alkoy, P. J. Alkoy and P. J. Kelly, Vacuum, 79 (2005) 221.
5 A. Chowdhuri, V. Gupta, K. Sreenivas, R. Kumar, S. Mozumdar and P. K. Patanjali, Appl. Phys. Lett., 84 (2004) 1180.
6 H. Cao and S. L. Suib, J. Am. Chem. Soc., 116 (1994) 5334.
7 Y. P. Wang, J. W. Zhu, X. J. Yang, L. Lu and X. Wang, Thermochim. Acta, 437 (2005) 106.
8 L. Bereczki, K. Marthi, P. Huszthy and G. Pokol, J. Therm. Anal. Cal., 78 (2004) 449.
9 Y. L. Su, S. F. Li and D. H. Ding, J. Therm. Anal. Cal., 86 (2006) 497.
10 J. Zhi, W. Tian-Fang, L. Shu-Fen, Z. Feng-Qi, L. Zi-Ru, Y. Cui-Mei, L. Yang, L. Shang-Wen and Z. Gang-Zhui, J. Therm. Anal. Cal., 85 (2006) 315.
11 Y. X. Luo, L. D. Lu, X. H. Liu, X. J. Yang and X. Wang, Chin. J. Inorg. Chem., 18 (2002) 1211.
12 N. B. Singh and A. K. Ojha, Thermochim. Acta, 390 (2002) 67.
13 V. R. Palkar, P. Ayyub, S. Chattopadhyay and M. Multani, Phys. Rev. B., 53 (1996) 2167.
14 Z. S. Hong, Y. Cao and J. F. Deng, Mater. Lett., 52 (2002) 34.
15 P. Ayyub, V. R. Palkar, S. Chattopadhyay and M. Multani, Phys. Rev. B., 51 (1995) 6135.
16 A. Punnoose, H. Magnone and M. S. Seehra, Phys. Rev. B., 64 (2001) 174420.
17 Y. Chang and H. C. Zeng, Cryst. Growth Des., 4 (2004) 397.
18 J. Boerio-Goates, G. S. Li, L. P. Li, T. F. Walker, T. Parry and B. F. Woodfield, Nano Lett., 6 (2006) 750.

19 L. J. Chen, G. S. Li and L. P. Li, Thermochim. Acta, in revision.
20 T. G. Cooper and N. H. de Leeuw, Langmuir, 20 (2004) 3984.
21 B. Lefez, R. Souchet, K. Kartouni and M. Lenglet, Thin Solid Films, 268 (1995) 45.
22 M. Lenglet and F. Hochu, Mater. Res. Bull., 32 (1997) 863.
23 S. Guha, D. Peebles and T. J. Wieting, Pys. Rev. B, 43 (1991) 13092.
24 Z. W. Wang, V. Pischedda, S. K. Saxena and P. Lazor, Solid State Commun., 121 (2002) 275.
25 J. F. Xu, W. Ji, Z. X. Shen and S. H. Tang, J. Solid State Chem., 147 (1999) 516.
26 R. P. Wang, G. W. Zhou, Y. L. Liu, S. H. Pan, H. Z. Zhang, D. P. Yu and Z. Zhang, Phys. Rev. B., 61 (2000) 16827.
27 V. V. Boldyrev, Thermochim. Acta, 443 (2006) 1.

Received: April 5, 2007
Accepted: June 5, 2007

DOI: 10.1007/s10973-007-8496-7